Macromolecules
ARTICLE

Macromolecules **2010**, *43*, 8379–8388 **8379**
DOI: 10.1021/ma1016242

Self-Organization of Coil−Ring−Coil Structures into Tubular Supramolecular Polymer Brushes: Synthesis, Morphology, and Growth

Martin Fritzsche,[†] Stefan-Sven Jester,*[,†] Sigurd Höger,*[,†] Christina Klaus,[‡] Nico Dingenouts,[‡] Peter Linder,[§] Markus Drechsler,[∥] and Sabine Rosenfeldt*[,⊥]

[†]*Kekulé-Institut für Organische Chemie und Biochemie, Rheinische Friedrich-Wilhelms-Universität Bonn, Gerhard-Domagk-Str. 1, 53121 Bonn, Germany,* [‡]*Institut für Technische Chemie und Polymerchemie, Karlsruhe Institut für Technologie, Engesserstr. 18, 76128 Karlsruhe, Germany,* [§]*Institut Laue-Langevin, BP 156, 6, rue Jules Horowitz, 38042 Grenoble Cedex 9, France,* [∥]*Institut für Makromolekulare Chemie II, Universität Bayreuth, Universitätsstr. 30, 95440 Bayreuth, Germany, and* [⊥]*Institut für Physikalische Chemie I, Universität Bayreuth, Universitätsstr. 30, 95440 Bayreuth, Germany*

Received July 20, 2010; Revised Manuscript Received September 5, 2010

ABSTRACT: Shape-persistent macrocycles based on the phenylene−ethynylene−butadiynylene backbone with extraannular amino groups were synthesized by the oxidative dimerization of the corresponding (BOC-protected) half-ring bisacetylenes. ABA block structures with a central rigid macrocycle and a flexible periphery (oligoalkyl and oligostyryl groups) were subsequently obtained by carbodiimide directed coupling of the macrocyclic diamines with the corresponding carboxylic acids. Depending on the solvent, an aggregation of the compounds toward tubular supramolecular polymer brushes could be induced. Cryogenic transmission electron microscopy and small-angle neutron scattering reveal the tubelike aggregates in solution. Atomic force microscopy confirms the morphology of these aggregates after casting onto surfaces. The aggregate growth occurs remarkably slowly. Solvophobic interactions—good solubility of the flexible substituents and weak solubility of the rigid macrocycle—combined with the oblate shape of the latter are determined as driving forces for the directed self-organization.

Introduction

Nanoengineering provides a top-down approach for the fabrication of micro- and nanoscale devices. While the spatial resolution of the corresponding lithographic processes is limited,[1,2] the complementary synthetic bottom-up approach provides a molecular strategy for the creation of smaller nanostructures.[3] In particular, the rational design of molecular building blocks, fulfilling specific requirements for spontaneous organization into nanoscale objects of decisive size, shape, and functionality, plays a key role in the concept of molecular self-organization.

One approach considers amphiphilic block copolymers as building blocks, known to assemble to superstructures in selective solvents. The design concept of an intramolecular combination of two or more chain segments of different chemical composition, expressing opposing solubility properties, has proven to be successful for the creation of such tailored superstructures.[4−7] Of particular interest for such objectives are rod−coil systems, consisting of a rigid and a flexible subunit.[8−10]

Nature presents various examples of complex structures created by self-assembly of small, well-defined molecules using noncovalent interactions.[11] One of the most detailed investigated biological superstructures is the tobacco mosaic virus (TMV) based on protein units around a viral RNA.[12] In that case the coat protein self-assembles into a rodlike, helical hollow superstructure with incorporated RNA protected in the cavity.[13] Several attempts have been made to mimic the aggregation and structure of the TMV or comparable nanoscale particles of defined size, shape, and functionality by synthetic building blocks with reduced complexity.[14] For the particular example of tubular structures, wedge-shaped dendrons can form superstructures that closely resemble the natural model.[15] Even a thermal change between different pore shapes has been reported in specifically designed systems.[16] On a similar size scale, a stately example from nature is the aggregation of the insulin molecule to protofibrils of 4−10 nm diameter and ∼200 nm length and subsequently to larger amyloid fibrillae, which are generally associated with diseases such as Alzheimer's disease, scrapie, Creutzfeldt−Jakob disease, and bovine spongiform encephalopathy (although the individual proteins vary with the respective disease).[17]

On the supramolecular size scale, recent studies involved atomic force microscopy (AFM) and transmission electron microscopy (TEM) of aggregates without[9,18−23] or with inner cavity (which may be empty or contain solvent or specific guest molecules).[24−30] A significantly different aggregation behavior of large molecular building blocks[17,31] as compared to small molecules[20,22,24−26,29] with respect to the time scale of aggregation is discussed. However, in both cases mostly nucleation−growth mechanisms have been discussed for the aggregation.

Shape-persistent macrocycles are predestined molecular structures for the anisotropic aggregation into tubular supramolecular structures. They can be functionalized at the interior as well as at the periphery, and their diameter can be adjusted. Thereby they serve as valuable model compounds to unravel the basic principles and requirements for the creation of tubular supramolecular objects in general. Tube formation can be obtained by specific intermolecular interactions between macrocycles, as for example in cyclopeptides[25,32] or cyclosaccharides,[33] or by nonspecific $\pi-\pi$ interaction or solvophobic forces, as mostly seen in π-conjugated macrocycles like in phenylene−ethynylene or phenylene−butadiynylene rings.[5,29−31,34,35] Aggregate formation can also

*Corresponding authors. E-mail: stefan.jester@uni-bonn.de (S.-S.J.); hoeger@uni-bonn.de (S.H.); sabine.rosenfeldt@uni-bayreuth.de (S.R.).

© 2010 American Chemical Society

Published on Web 09/29/2010

be induced by salt addition.[24,36] Moreover, it must be pointed out that such superstructures are interesting candidates for advanced and fast chemical sensors[37] or may function as templates for the formation of metal nanorods.[38]

It turned out that the attractive forces between aromatic macrocycles strongly depend on the ring substituents. If the solvent quality is kept constant, electron-poor compounds show a much higher tendency to aggregate than electron-neutral or electron-rich compounds. In addition, bulky substituents hinder an aggregation.[39,40] Nevertheless, even macrocycles with large side groups can form extended aggregates in solution if the environment is a nonsolvent for the rigid core of the compounds (solvophobic aggregation), and sufficient compound solubility is provided.

Recently, we investigated shape-persistent macrocycles with extraannular oligoalkyl[30] or oligostyryl/polystyryl[35] side chains as molecular building blocks to obtain such tubular superstructures. Aggregates of the latter can be viewed as tubular supramolecular polymer brushes.[41c,42] Tube formation is based on the intramolecular combination of a planar, shape-persistent backbone, exhibiting low solubility and, elementarily, pretending a preferred (but not exclusive) growth in one direction, and the oligoalkyl or oligostyryl/polystyryl (PS) side chains, assuring sufficient solubility, and shaping a protective matrix around the tubes. The diameter and functionality of the macrocyclic backbone are the subject of rational molecular design via covalent bond chemistry.[43] All these channel structures are in close analogy to rod−coil systems, in which microphase separation and the formation of ordered structures can be obtained even at rather low degrees of polymerization due to a larger Flory−Huggins χ parameter.[10c,d] We also investigated the growth kinetics of a coil−ring−coil block structure, which have pointed out being slow and temperature dependent (where aggregation occurs faster at lower temperatures).[35d] The aggregation process shows all characteristics of a cooperative self-organization.[36,37,44]

Besides the challenge of evolving novel synthetic strategies for the extraannular substitution of the macrocycles, the aforementioned results motivated us to find analogue systems providing solvent- and temperature-dependent aggregation behavior, thus supporting the generality of our design principle to achieve tubular structures. Furthermore, we were particularly motivated to improve the microscopic insight on the aggregation process as well as getting a clearer knowledge about the final aggregate morphology.

Here we describe the synthesis and characterization of amine-functionalized shape-persistent phenylene−ethynylene−butadiynylene macrocycles and their incorporation into coil−ring−coil block structures with oligostyrene (**1a**, **2a**) and oligoalkyl side chains (**1b**, **2b**) (Scheme 4) containing additional amide moieties. In the first part of investigations, shape, size, and bundling behavior of anisotropic aggregates of this system are investigated *in situ* by dynamic light scattering (DLS), small-angle neutron scattering (SANS), and (cryo-) TEM. In a second part, we confirm the aggregate shape and stability in air by AFM after deposition of the respective nanotubes onto surfaces and focus on the morphologies of different aggregate growth stages.

Experimental Part

Synthesis. Details on the synthesis and characterization of all new compounds are given in the Supporting Information.

Instruments and Characterization. *Dynamic Light Scattering* (*DLS*). Light scattering experiments were carried out with an ALV/CGS 3 compact goniometer system connected to an ALV/LSE-5004 light scattering electronics and multiple tau digital correlator. Data treatment was performed as described in ref 45.

Small-Angle Neutron Scattering (*SANS*). The macrocycle **2a** was dissolved in deuterated cyclohexane (10.0 g/L, Deutero GmbH, deuteration grade 99.5%). To induce complete solubility, the sample was heated for a few minutes to about 50 °C. All SANS data were taken at 25 °C using the instrument D11 at the Institut Laue-Langevin (ILL) in Grenoble, France, providing 0.6 nm wavelength. Sample−detector distances of 1.1, 5.0, and 17.0 m were used. Radially averaged intensities in absolute scale were obtained using the software provided with the instrument. Further data treatment was done according to ref 46. A detailed analysis of the data is given in the Supporting Information.

Transmission Electron Microscopy (*TEM*). For TEM measurements, the macrocycle **2a** was dissolved in cyclohexane at room temperature to yield a concentration of 0.6 wt %. The measurements were performed after heating the sample to ca. 50 °C for some minutes and subsequently cooling down to room temperature again. A carbon-coated TEM grid was dipped into the solution and subsequently air-dried. The sample was transferred into a Zeiss EM 922 OMEGA EFTEM (operated at 200 keV). Data acquisition was performed using a CCD camera system (Ultrascan 1000, Gatan) connected to a digital image processing system (Gatan Digital Micrograph 1.8.2).

Cryogenic Transmission Electron Microscopy (*Cryo-TEM*). For cryo-TEM measurements, the macrocycle **2a** was dissolved in cyclohexane at room temperature to yield a concentration of 0.4 wt %. The measurements were performed after heating the sample to ca. 50 °C and subsequent cooling to room temperature. Further sample preparation included casting the solution onto a lacey carbon film, instant vitrification by immersing the sample into liquid nitrogen (Zeiss Cryobox freezing unit, Zeiss NTS GmbH, Oberkochen, Germany), and subsequent transfer (cryo-transfer sample mount CT3500, Gatan, München, Germany) into a Zeiss EM 922 OMEGA EFTEM (operated at 200 keV). The sample was held at ca. −175 °C during the whole microscopy measurement. Data acquisition was performed using a CCD camera system (Ultrascan 1000, Gatan) connected to a digital image processing system (Gatan Digital Micrograph 1.8.2).

Atomic Force Microscopy (*AFM*). Atomic force microscopy was applied to investigate aggregates of **2a**, supported on mica and highly oriented pyrolytic graphite (HOPG) substrates. In a first experiment, a 10^{-3} M solution was used as prepared at rt, and the thick film drop-cast from a 4 h old solution was investigated after applying and drying a droplet onto HOPG. For detailed investigations, 10^{-3}, 10^{-4}, 10^{-5}, and 10^{-6} M solutions of **2a** in cyclohexane (99.9% purity, Sigma-Aldrich) were initially heated to 60 °C for 15 min to induce complete dissociation of all aggregates, subsequently cooled to 10 ± 2 °C, and stored at this temperature for several days. The progress of aggregate growth was investigated at different growth times by depositing the materials onto substrates by dip-coating (mica) or drop-casting (HOPG), drying in air, and subsequent AFM measurement. Note that no coagulation or opacity of the solution was observed, even at the highest concentration used.

AFM measurements were performed using an Agilent 5500 Pico Plus system, operated in tapping mode under ambient conditions (air, room temperature). DP15/GP cantilevers (Mikromasch, specified tip radius 10 nm, nominal spring constant 40 N/m) were used. The measurements were performed with cantilever oscillation amplitudes near the lower (sticking) threshold to yield highest resolution (near tip radius limit). All AFM images were recorded within 3 h after sample preparation. The software package SPIP (Image Metrology) was used for further processing of the images.

Muscovite mica was obtained from Plano, Wetzlar. HOPG was used in SPI-2 grade quality (Structure Probe, Inc.). Mica and HOPG substrates were freshly cleaved before use. Step edge densities for HOPG substrates are typically 1−10 μm^{-1} with step heights from 1 monolayer (ML, 0.34 nm) to several 10 nm with an average height of a few ML.

Results and Discussion

Synthesis. 3-(3,5-Diiodophenoxy)propylphthalimide (**5**) is obtained by Williamson ether coupling of **3** and **4**. After deprotection with hydrazine the free amine **6** is treated with

Scheme 1.[a]

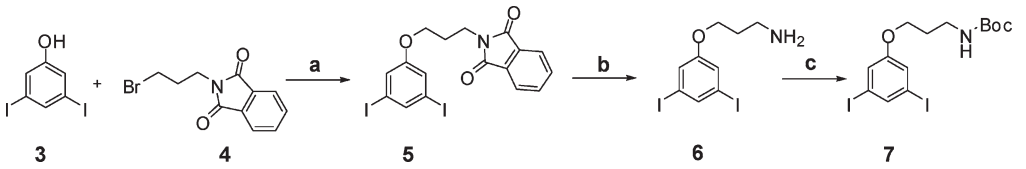

[a] Reagents and conditions: (a) K_2CO_3, DMF, 70 °C, 83%; (b) 1: $H_4N_2 \times H_2O$, ethanol, reflux; 2: HCl, rt; 3: NaOH, rt, 93%; (c) di-*tert*-butyldicarbonate, Et_3N, DMF, rt, 88%.

Scheme 2.[a]

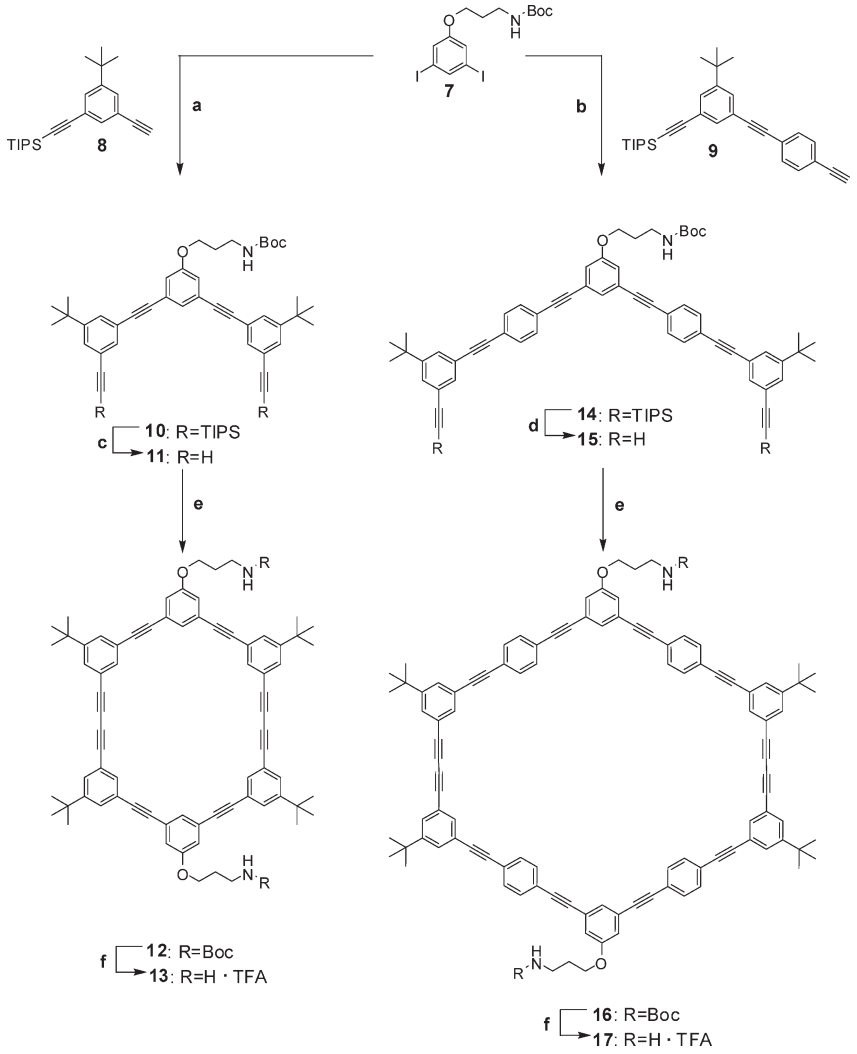

[a] Reagents and conditions: (a) $Pd(PPh_3)_2Cl_2$, PPh_3, CuI, THF/NEt_3, 50 °C, 18 h, 76%; (b) $Pd(PPh_3)_2Cl_2$, PPh_3, CuI, THF/NEt_3, rt, 18 h, 85%; (c) TBAF, THF, rt, 18 h, 79%; (d) TBAF, THF, rt, 18 h, 80%; (e) CuCl, $CuCl_2$, pyridine, rt, 96 h + 48 h, 43% (**12**) and 20% (**16**), (f) TFA, CH_2Cl_2, rt, 18 h, 80% (**13**) and 92% (**17**).

Boc_2O in order to get the target structure **7** (Scheme 1).[47] Attempts to use **5** or **6** directly for the macrocycle synthesis were not successful; no pure coupling product could be isolated. The synthesis of the amine-functionalized macrocycles **13** and **17** is displayed in Scheme 2. Starting from the Boc-protected amine **7**, the half-rings **11** and **15** were obtained by Pd-catalyzed Sonogashira−Hagihara coupling with **8**[48] and **9**,[35] respectively, and subsequent desilylation of **10** and **14** with Bu_4NF. The macrocyclic structures **12** and **16** were synthesized by CuCl/$CuCl_2$-promoted coupling of the half-rings **11** and **15** under pseudo-high-dilution conditions and purified by column chromatography. The purity of the rings was determined by NMR spectroscopy, mass spectrometry, and, most importantly, by gel permeation chromatography (GPC) to exclude the presence of trimers and higher oligomers. Acid-catalyzed deprotection generated the macrocyclic diamines **13** and **17**. PS-COOH (**18**) was obtained by anionic polymerization of styrene (initiated by *sec*-BuLi) and reaction with CO_2.[35c] For the synthesis of a PS block with an additional amide moiety, PS-COOH (**18**) was coupled with β-alanine methyl ether hydrochloride and deprotected to obtain the carboxyl-functionalized polystyrene **20** (Scheme 3). The dendritic carboxylic acid **26** was obtained as a white solid from methyl-3,5-dihydroxy benzoate (**21**) by alkylation with **22** and subsequent base-catalyzed deprotection, EDC promoted coupling with β-alanine methyl ether

Scheme 3.[a]

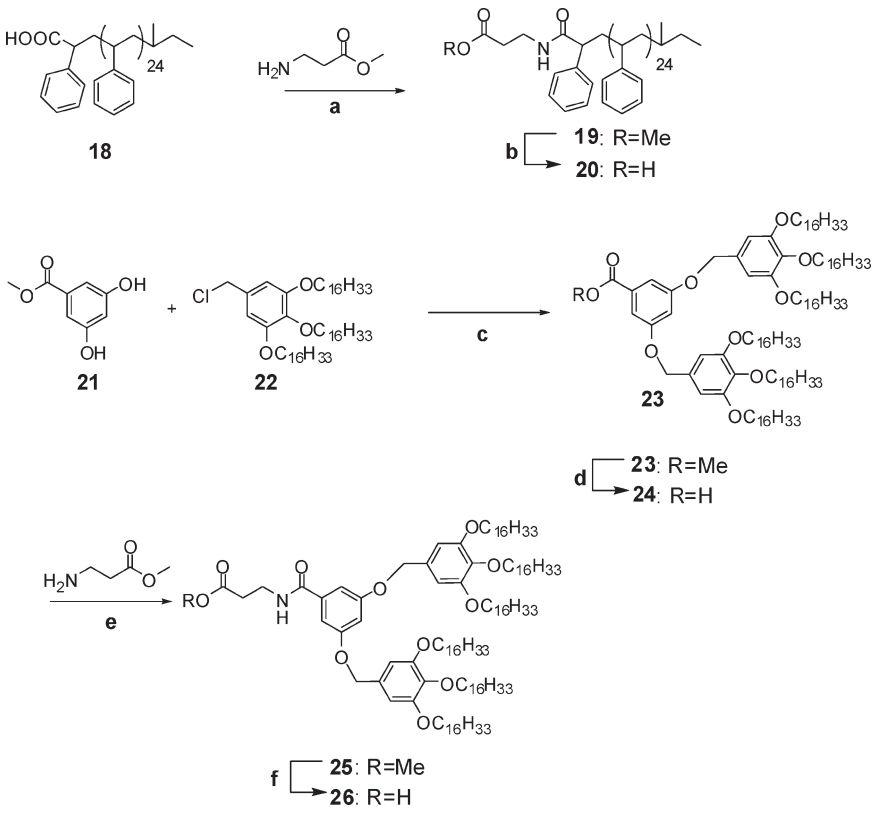

[a] Reagents and conditions: (a) β-alanine methyl ether hydrochloride, *N*-(3-dimethylaminopropyl)-*N*′-ethylcarbodiimide, DMAP, dichloromethane, DMF, rt, 18 h; 85%; (b) 1: KOH_{aq} (10%), reflux, 18 h; 2: HCl (conc)/H_2O (1:1, v/v), rt, 30 min; quant; (c) K_2CO_3, DMF, 70 °C, 68%; (d) 1: KOH_{aq} (10%), reflux, 18 h; 2: HCl (conc)/H_2O (1:1, v/v), rt, 30 min, 97%; (e) β-alanine methyl ether hydrochloride, *N*-(3-dimethylaminopropyl)-*N*′-ethylcarbodiimide, DMAP, dichloromethane, rt, 48 h, 91%; (f) 1: KOH_{aq} (10%), reflux, 18 h; 2: HCl (conc)/H_2O (1:1, v/v), rt, 30 min, 76%.

hydrochloride to **25** and saponification of the ester by treatment with aqueous KOH in THF.

PS-COOH (peak molecular weight M_P = 2500 g/mol) **18**[35] and 3,4,5-tris(dodecyloxy)benzoic acid **27**[49] were attached to the diamine **13** by carbodiimide-promoted coupling in dichloromethane (Scheme 4) to yield the pure target structures **1a** (after column chromatography) and **1b** (after column chromatography and subsequent purification by preparative GPC in THF). Coupling of **17** with carboxylic acids **20** and **26** yielded compounds **2a** and **2b** (Scheme 4). The crude reaction products were purified by column chromatography and preparative GPC in THF to obtain the pure products as white powders. All macrocyclic systems are soluble in dichloromethane, chloroform, and THF and were characterized by NMR spectroscopy, GPC, and mass spectrometry (Maldi-MS).

Aggregation in Solution. As mentioned in the Introduction, the aggregation of rigid macrocyclic compounds is strongly solvent-dependent. In THF as well as aromatic and chlorinated solvents all macrocyclic compounds **1** and **2** do not show any indications of an aggregation. However, aggregation to tubelike superstructures might be induced—as previously successfully shown[50]—by adding a solvent solubilizing specifically the flexible side chains and acting as a nonsolvent for the rigid core, e.g., cyclohexane. Concentration-dependent measurements of the proton NMR spectra of **1b** in dichloromethane/cyclohexane (1:3, v/v) indicate that aggregation and dissociation are fast on the NMR time scale (Figure 1). Assuming that the monomer−dimer equilibrium is the predominant process in solution, we obtained a dimerization constant, K_{assoc}, of 40 ± 10 M^{-1} in CD_2Cl_2/cyclohexane-d_{12} (1:3 at 25 °C).[51] This value is in the same range as previously reported data on similar compounds in a similar environment.[50] However, a further polarity decrease of the solvent system by increasing the volume fraction of cyclohexane is not possible due to the limited solubility of **1b**.

On the other hand, more bulky side groups guarantee that compound **2b** as well as block copolymers **1a** and **2a** are soluble in pure cyclohexane. The complex signals in the aromatic region of the proton NMR did not allow the determination of the association constant by concentration-dependent NMR measurements. Therefore, dynamic light scattering experiments of **1a**, **2a**, and **2b** were carried out in cyclohexane and dichloromethane. As expected from proton NMR spectra, dynamic light scattering measurements of the compounds in dichloromethane reveal a hydrodynamic radius of about 2 nm. This can be associated with the free nonaggregated macrocycles. However, the CONTIN analysis[52] of the autocorrelation function of **1a** in cyclohexane gives a bimodal distribution of the relaxation times, representing hydrodynamic radii of about 2−3 nm and about 100 nm (Figure 2a). A similar result is obtained for **2a** (Figure 2b). Contrary, for **2b** we observed also in cyclohexane a monomodal size distribution at around 4 nm (Figure 2c).[53] Recent investigations[35c,d] on a PS−macrocycle−PS structure with oligostyrenes attached via ester linkage have shown that those compounds strongly aggregate in cyclohexane to form extended fibers. Therefore, a considerably stronger aggregation was expected for **2a** since it contains the same core and corona structure but additional polar sites amenable to form hydrogen bonds. However, even at concentrations above 1 wt % no apparently unusual increase of the solution viscosity could be observed. **2a** does not form a gel in cyclohexane at 1 wt % concentration. The expected stronger aggregation compared to the compound investigated in ref 35d—due to

Scheme 4.[a]

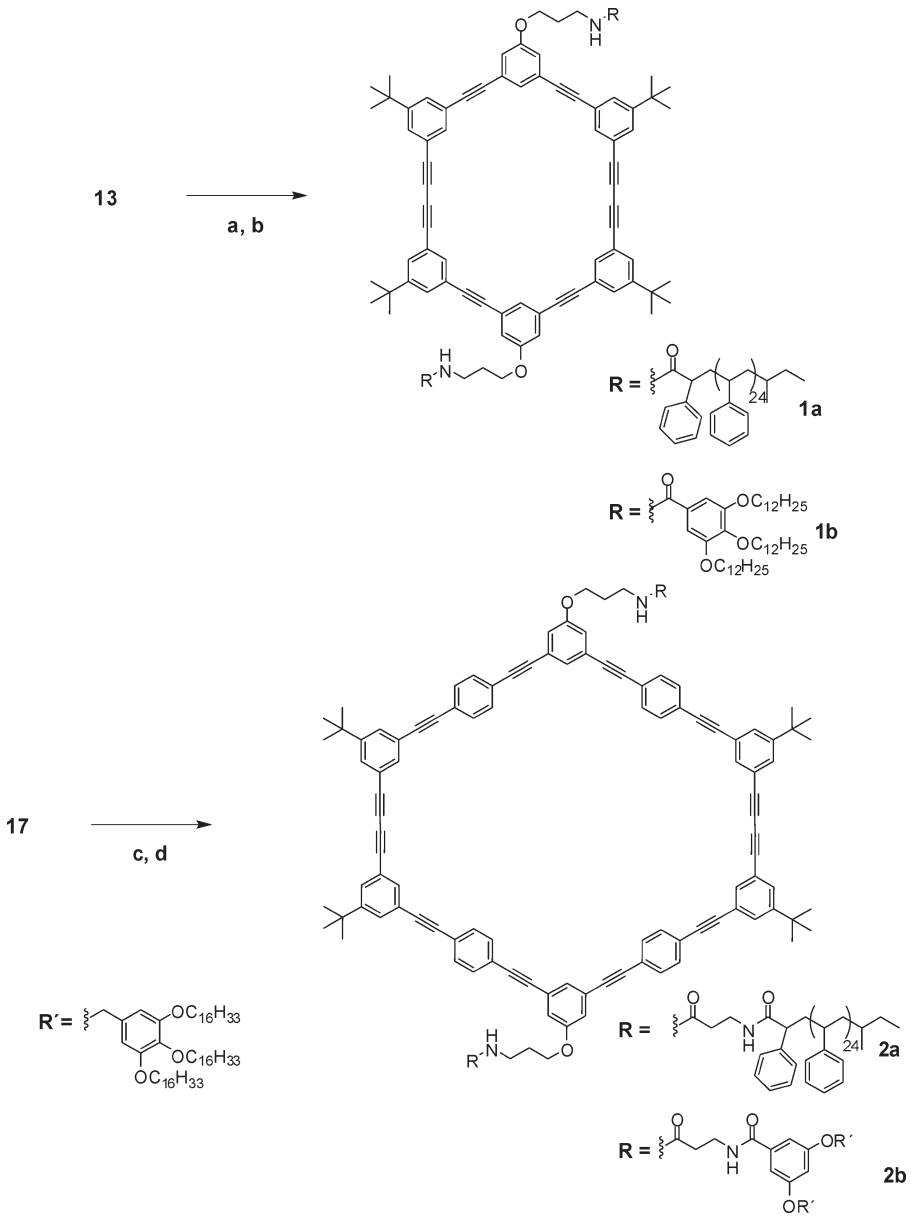

[a] Reagents and conditions: (a) **18**, DMAP, diisopropylcarbodiimide, dichloromethane, rt, 48 h, 57%; (b) **27**,[49] DMAP, diisopropylcarbodiimide, dichloromethane, rt, 48 h, 29%; (c) **20**, DMAP, *N*-(3-(dimethylamino)propyl)-*N*′-ethylcarbodiimide, chloroform, rt, 18 h, 37%; (d) **26**, DMAP, diisopropylcarbodiimide, dichloromethane, rt, 48 h, 28%.

the additional peptide unit, allowing the formation of intermolecular hydrogen bonds—could be observed in none of the cases. This shows that the enthalpic and entropic balance within the aggregate formation is difficult to predict.

Nevertheless, to yield information about supramolecular aggregates in solution, small-angle neutron scattering (SANS) measurements were performed. **2a** was dissolved in d_{12}-cyclohexane to enhance the contrast. The scattering intensity $I(q)$ as a function of the scattering vector q of **2a** exhibits the typical scaling behavior of q^{-1} for randomly orientated rods.[54] The evaluation of the corresponding q-range yields a radius of gyration perpendicular to the cylinder axis of $R_c = 4.1$ nm[55] and a mass per unit length of $M_L = 3.14 \times 10^4$ g/mol/nm, or 4.5 molecules per nm, leading to the assumption of a 2.2 Å stacking distance, respectively. A previous X-ray investigation of a crystalline phase of tubular aligned macrocycles yielded an average stacking distance of 6.2 Å,[35c] and significantly smaller distances seem very unlikely. Thus, the average number of single molecules per nanometer as well as the cross-sectional radius can only be explained if bundling of the cylindrical tubes is assumed (see Supporting Information for further details). On the basis of our previous results on similar systems, the SANS data were simulated applying different models of cylindrical structures. It turned out that the simple model of a polydisperse homogeneous cylinder is sufficient to simulate the data (cf. discussion in Supporting Information). Figure 3 shows experimental and simulated data. The best description was achieved for a cylinder with a length of $L = 65$ nm and a radius of $R = 4.7$ nm.[55] At higher scattering angles, thermal density fluctuations of the side chains have to be taken into account. In a simple approximation this can be done by adding a constant or, as done here, a Gaussian to the scattering intensity.[54] Both contributions lead to a good description of the data, as supported by AFM and cryo-TEM results. Thus, by SANS we proved the presence of cylindrical aggregates in 1 wt % solutions of **2a** in cyclohexane at room temperature.

TEM as well as cryo-TEM images obtained from 0.4−0.6 wt % (~4.5×10^{-4}−7×10^{-4} M) solutions of **2a** in cyclohexane reveal the presence of 30−250 nm long fiber-shaped aggregates. The strong intermolecular interactions provide sufficient stability for transferring the aggregates onto the lacey carbon film substrate for cryo-TEM. Aggregate tubes of 8−12 nm diameter (Figure 4a, marked with arrows), as well as thicker bundles of several aggregates, up to 50 nm wide (arrow in Figure 4b), are observed, in some cases fibers with a bandlike or drilled structure.

Further support for the presence of the tubelike aggregates resulted from AFM investigations. **2a** was drop-cast from a 10^{-3} M (0.9 wt %) solution in cyclohexane onto mica and HOPG substrates and subsequently investigated by intermittent contact mode AFM. The resulting several nanometer thick film exhibited a rough hill surface structure (as expected for thick films of organic materials), but also a clearly visible substructure of domains of densely packed nearly parallel oriented stripes of anisotropic aggregates of **2a** with 60 ± 20 nm length and 13 ± 3 nm tube−tube distances (see Figure 5a,b), yet in good coincidence with SANS and (cryo-) TEM results.

The slow, temperature-dependent aggregation process of similar ring−coil structures via nuclei to tubes, as previously reported,[35d] has hitherto been quantified in magnetic birefringence measurements. This motivated us to complementarily investigate the morphology of individual aggregates (of **2a**) at different growth stages by AFM, as AFM results are so far still limited to the observation of fully grown tube-shaped aggregates cast from sufficiently long stored solutions. This would yield a more detailed insight on the different shapes and sizes of intermediates during the growth process. A solution of **2a** (10^{-5} M, 0.009 wt %) was heated to 60 °C, clearly above the dissociation threshold, and then rapidly cooled to 10 °C. After storing the solution at this temperature for different time periods, the different particle sizes and shapes determined by AFM (after casting onto a substrate) reflect the different growth stages (nucleation and elongation) of the aggregates of **2a** in cyclohexane (Figures 6 and 7 on mica and HOPG, respectively). On mica, after 5:30 and 21 h (Figure 6, a and b, respectively) few anisotropic tube-shaped aggregates (height 6 ± 0.5 nm) of **2a** can be found in a matrix consisting of monomers and isotropic aggregates. During the reorganization process in solution, the surface coverage by a 1.5 nm thin film—as observed on mica and attributed to monomers—decreases with time due to the increasing order of the molecules within the growing aggregates (holes in the monomer film are marked by arrows in Figure 6a). While the formation of the isotropic aggregates is fast, the aggregate sizes and shapes still change on a longer time scale of a few days; e.g., Figure 6c displays the aggregates after 8 days. Finally, after 14 days (Figure 6d), strongly anisotropic rods with an aspect ratio of ~10, a length of

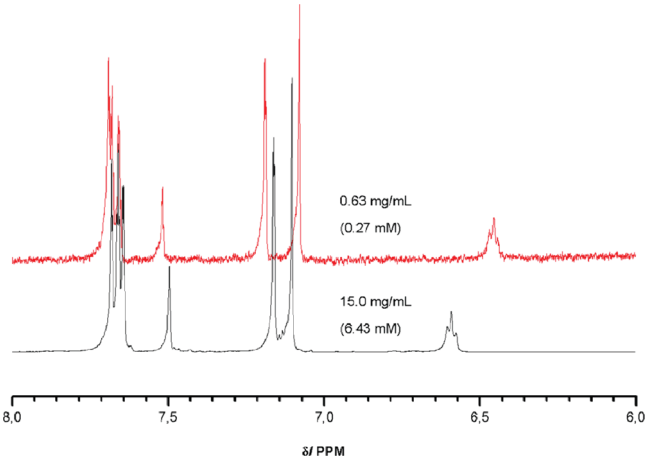

Figure 1. Concentration dependence of ^{1}H NMR spectra (400 MHz) of **1b** in CD_2Cl_2/cyclohexane-d_{12} (1:3) at room temperature.

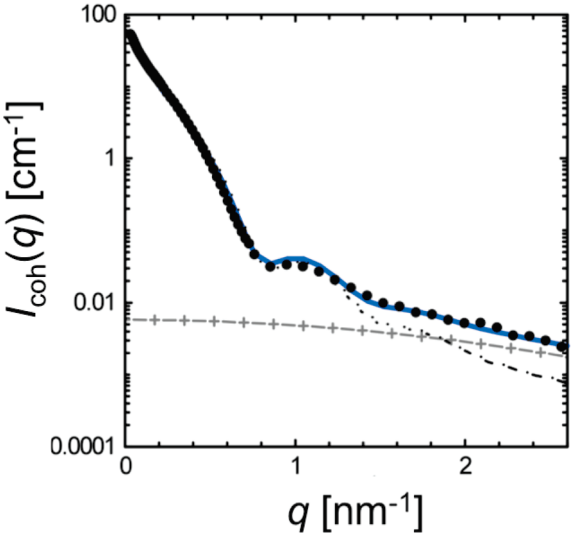

Figure 3. Modeling of the cylindrical aggregates. The coherent scattering intensity of aggregates of **2a** (10 g/L, in deuterated cyclohexane, ● symbols) is compared with the calculated intensity of polydisperse homogeneous cylinders (-·- line, length L = 65 nm, radius R = 4.7 nm, estimated standard deviation of the radius σ_R = 12%). To account contributions due to density fluctuation of the side chains, a Gaussian has been added to the theoretical intensity of the polydisperse homogeneous cylinder (− + − line). Considering both contributions yields a good description (solid blue line) of the experimental data.

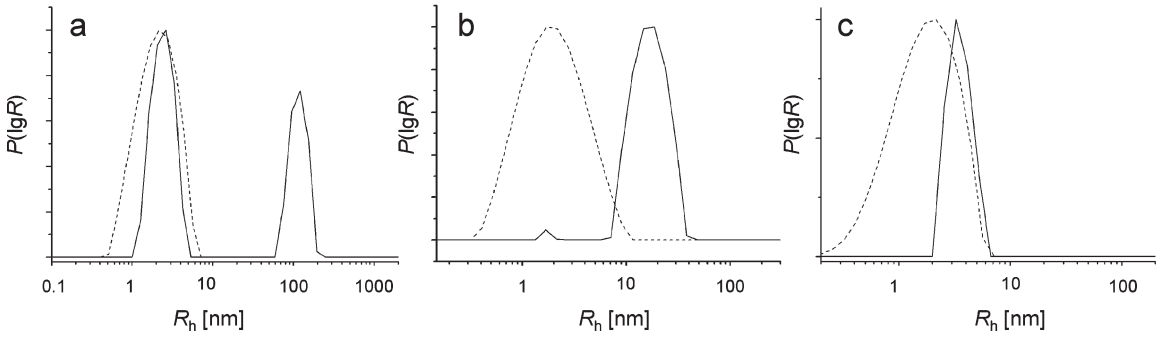

Figure 2. CONTIN fit: distribution of DLS relaxation times of (a) **1a**, (b) **2a**, and (c) **2b** in dichloromethane (---) and cyclohexane (—) at a concentration of 0.08 wt % at 20 °C.

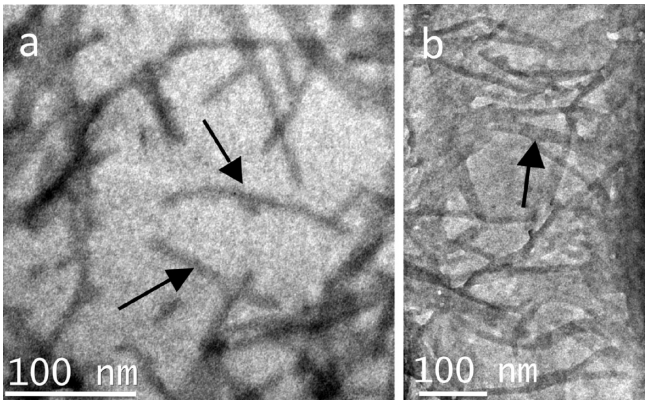

Figure 4. (a) TEM and (b) cryo-TEM micrographs of unstained tube-shaped aggregates of **2a** formed in cyclohexane (a: 0.6 wt %, $\sim 7 \times 10^{-4}$ M; b: 0.4 wt %, $\sim 4.5 \times 10^{-4}$ M).

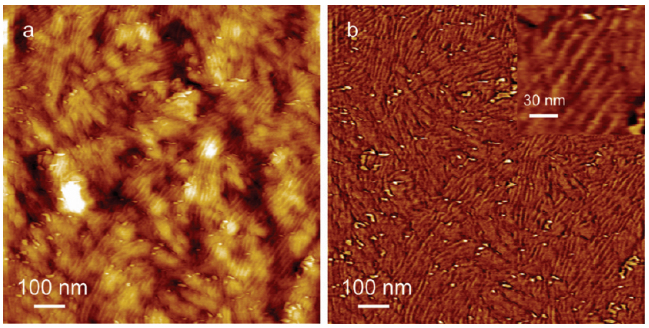

Figure 5. AFM images of a thick film, cast from a 10^{-3} M solution of **2a** onto HOPG. (a) Topography raw data. (b) Topography data after deconvolution from the hill structure, enhancing the visibility of features in the < 20 nm size regime.[56]

$\sim 60 \pm 20$ nm, and a height of about $\sim 6 \pm 0.5$ nm are observed. Noteworthy, the formation of anisotropic aggregates of **2a** is significantly slower than reported for smaller molecules,[20,22,24–26,29] and a fast formation of isotropic aggregates—which are already visible after few hours—precedes the slow growth of the tubular aggregates as also previously reported on a similar system.[35d] The observed heights of 6 ± 0.5 nm as well as the observed lengths of the tube structures are coincident with the results of the TEM/cryo-TEM experiments. This again allows the conclusion that the tubelike structures shown here are built by macrocycles with their backbone oriented perpendicularly to the substrate. The tubes appear in network structures, and no individual tubes are observed. During the casting process, the particles are sufficiently mobile to form the aggregates (and bundles).

On HOPG a similar growth scenario with an initial observation of small isotropic aggregates and subsequent slow formation of tubes is observed.[57] Figure 7a shows small isotropic particles, which have grown within 1 h. After 68 h (Figure 7b), tubelike features are visible. Contrarily to the adsorption on mica, on HOPG most of the aggregates (on the atomically flat terraces) are laterally well separated (but still with accidental neighbor contact), and step edges boost a bundle formation (see Supporting Information)—possibly an effect of dewetting during the casting procedure. Although a mean width of 20 nm is detected for the anisotropic 6 nm high aggregates in Figure 7b–e, the lateral dimensions of such small features are typically overestimated due to tip convolution.[58,59] Additionally, in some cases (as pointed out in Figure 7d, which is a detail image of Figure 7c

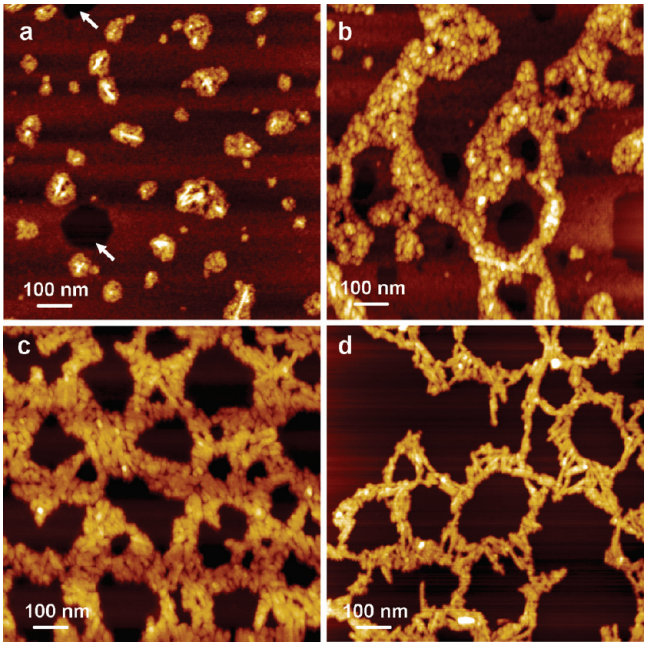

Figure 6. AFM images of aggregates, cast from a 10^{-5} M (0.009 wt %) solution of **2a** in cyclohexane (kept for different times at 10 °C) onto mica. (a) After 5:30 h, very few small tube-shaped aggregates of 70 ± 15 nm length and 6 ± 0.5 nm height (above a thin film) are observed, embedded in a matrix of smaller, isotropic particles. The surface is covered with a rough (0.12 nm roughness average) 1.5 nm thin film (as measured with respect to the holes ($\sim$3% of overall surface area, marked by arrows), attributed to monomers (proposably with macrocycle backbones aligned parallel to the substrate)). (b) 21 h after initiation, the surface is mainly covered by isotropic nuclei ($h = 5.5 \pm 1.5$ nm, 40% coverage) on the cost of the monomeric film (thickness 1.5 nm, 50% coverage). (c) After 8 days, a network of 40 ± 20 nm long tube-shaped particles with a uniform height of 6 ± 0.5 nm is observed, and after 14 days (d), the length has slightly increased to 60 ± 20 nm. The smallest distinguishable tube–tube distances (of parallel tubes) are $\sim$12 nm.

with decreased *z*-scale) the tubes are lying on a monolayer of densely packed stripes with a height of 2 Å and a periodicity of 6 ± 0.2 nm. We attribute the latter to a self-assembled monolayer of 1D aligned flat-lying macrocycles (i.e., macrocycle backbones parallel to HOPG surface), which exhibit lateral phase separation where stripes of backbones appear to be separated by stripes containing the PS side chains (compare model shown in Figure 7f).[60] Conclusively, we assume that the anisotropic features in Figure 7b–e are individual tubes of **2a** and bundles of a few parallel-aligned tubes (which are undistinguishable by AFM).

The different adsorption behavior of aggregates of **2a** on HOPG and mica (under otherwise similar conditions) can be drawn back onto unlike adsorbate–substrate interactions with the respective substrates. The interaction of nonpolar organic materials with polar surfaces such as mica is lower than the strength of the aggregate–aggregate interaction; thus, a network formation is energetically favorable. Contrary, the interaction of (nonpolar) HOPG with aggregates of **2a** is higher or at least in the range of the adsorbate–adsorbate interaction. This is expressed by the adsorption of well-separated individual aggregates and bundles hereof as well as the formation of a self-assembled monolayer of individual coil–ring–coil molecules.[61] Conclusively, the network formation tendency is significantly influenced by the substrate. Nevertheless, the visualization of *individual* tube-shaped objects (and defined aggregates of tubes, here denoted as bundles) was possible from sufficiently dilute solutions. In addition, our time-dependent measurements

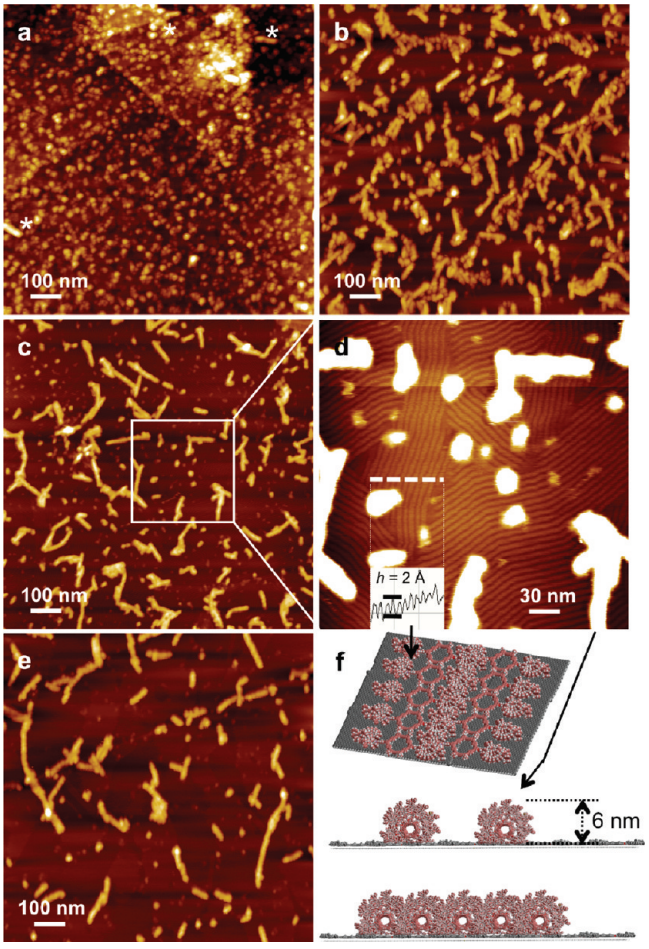

Figure 7. AFM images of aggregates, cast from a 10^{-5} M (0.009%) solution of **2a** from cyclohexane onto HOPG. (a) After 1 h, the substrate is covered by 3 ± 1 nm high anisotropic particles (while already few ~50 nm long rods are observed, marked by an asterisk). (b) After 68 h, the amount of tubes has significantly increased. (c) After 8 days, < 20−150 nm long tubes of 6 ± 0.5 nm uniform height, as well as small isotropic particles of ~1 nm height, are observed. (d) is a magnification of the marked region in (c). The inset is a topography cross section of the dashed white line. Remarkably, between the 6 nm high bright features, parallel stripes with a height of 2 Å and a periodicity of 6.0 ± 0.2 nm are observed, appearing in domains of ~100^2 nm^2 size with respect to differing alignment directions (while within a domain, bending of < 20° occurs). (e) A similar aggregate morphology is observed after 18 days (including stripes as in (d)). (f) A model representing the self-assembled monolayer discussed in (d), and two side-view models of the tubular aggregates (individual tubes and bundle) are shown.

clearly show that the aggregation of oligostyrene-decorated shape-persistent macrocycles is not a simple process in which the final ordered tubelike structure is directly formed from its constituents. Rather, an aggregation occurs toward an unstructured aggregate, which then reorganizes to build up the supramolecular hollow cylinders, which—again—form bundles of cylinders. The same behavior could recently be investigated by magnetic birefringence for the coil−ring−coil structure in which the different blocks were glued together by ester bonds. Therefore, our present study is complementary to our previous communication.[35d]

Conclusion

On the basis of the BOC protection of the amine functionality, we could perform $CuCl/CuCl_2$-mediated bisacetylene coupling to prepare two different shape-persistent macrocycles, each containing two extraannular amine groups. These were coupled with oligostyrene (leading to coil−ring−coil block systems) and oligoalkyl side chains. An aggregation was observed by NMR measurements and DLS. One coil−ring−coil structure, **2a**, was investigated in detail, and SANS supports the existence of polymer brushes by showing long cylindrical supramolecular aggregates with the diameter of approximately one molecule. (Cryo-) TEM confirms this observation. AFM measurements gave a deeper insight into the kinetics of the aggregate formation. It starts with the formation of small, isotropic aggregates, while anisotropic growth or organization is slower. These investigations are complementary to our previously reported kinetic studies on a similar system that were undertaken in solution.[35d] Further investigations will—on the surface—involve methods of nanostructured deposition of PS−ring−PS nanotubes onto patterned substrates as well as—in solution—further modification to explore the generality of this behavior for other coil−ring−coil systems.

Acknowledgment. Financial support by the Deutsche Forschungsgemeinschaft (DFG) and the SFB 624 is gratefully acknowledged. We gratefully acknowledge beam time at the instrument D11 at the ILL, Grenoble.

Supporting Information Available: Further details on the investigation of **2a** (SANS and AFM) plus the synthetic procedures and characterization of all compounds not previously described. This material is available free of charge via the Internet at http://pubs.acs.org.

References and Notes

(1) Waser, R. *Nanoelectronics and Information Technology: Materials, Processes and Devices*, 2nd ed.; Wiley-VCH: Weinheim, 2005.
(2) Rai-Choudhury, P., Ed.; *Handbook of Microlithography, Micromachining and Microfabrication*; Institution of Engineering and Technology: London, 2004; Vols. *1* and *2*.
(3) Ozin, G. A.; Arsenault, A. C.; Cademartiri, L. *Nanochemistry*, 2nd ed.; RSC Publishing: London, 2009.
(4) Alexandridis, P.; Lindman, B. *Amphiphilic Block Copolymers*; Elsevier Science B.V.: Amsterdam, 2000.
(5) (a) Lee, M.; Jeong, Y.-S.; Cho, B.-K.; Oh, N.-K.; Zin, W.-C. *Chem. Eur. J.* **2002**, *8*, 876–883. (b) Ryu, J.-H.; Oh, N.-K.; Lee, M. *Chem. Commun.* **2005**, 1770–1772. (c) Kim, J.-K.; Lee, E.; Kim, M.-C.; Sim, E.; Lee, M. *J. Am. Chem. Soc.* **2009**, *131*, 17768–17770.
(6) Tang, C.; Lennon, E. M.; Fredrickson, G. H.; Kramer, E. J.; Hawker, C. J. *Science* **2008**, *322*, 429–432.
(7) Yu, H.; Kobayashi, T. *Molecules* **2010**, *15*, 570–603.
(8) Reviews about rod−coil block copolymers: (a) Lee, M.; Cho, B.-K.; Zin, W.-C. *Chem. Rev.* **2001**, *101*, 3869–3892. (b) Klok, H.-A.; Lecommandoux, S. *Adv. Mater.* **2001**, *13*, 1217–1229. (c) Mao, G.; Ober, C. K. *Acta Polym.* **1997**, *48*, 405–422.
(9) (a) Zubarev, E. R.; Pralle, M. U.; Li, L.; Stupp, S. I. *Science* **1999**, *283*, 523–526. (b) Zubarev, E. R.; Pralle, M. U.; Sone, E. D.; Stupp, S. I. *J. Am. Chem. Soc.* **2001**, *123*, 4105–4106.
(10) For some recent examples of complex superstructures formed by rod−coil block copolymers see, for example: (a) Halperin, A. *Macromolecules* **1990**, *23*, 2724–2731. (b) Chen, J. T.; Thomas, E. L.; Ober, C. K.; Mao, G.-P. *Science* **1996**, *273*, 343–346. (c) Jenekhe, S. A.; Chen, X. L. *Science* **1999**, *283*, 372–375. (d) Klok, H.-A.; Langenwalter, J. F.; Lecommandoux, S. *Macromolecules* **2000**, *33*, 7819–7826. (e) Engelkamp, H.; Middelbeek, S.; Nolte, R. J. M. *Science* **1999**, *284*, 785–788. (f) Raez, J.; Manners, I.; Winnik, M. A. *J. Am. Chem. Soc.* **2002**, *124*, 10381–10395.
(11) (a) Whitesides, G. M.; Mathias, J. P.; Seto, C. T. *Science* **1991**, *254*, 1312–1319. (b) Lehn, J.-M. *Supramolecular Chemistry*; VCH: Weinheim, 1995.
(12) (a) Klug, A. *Angew. Chem.* **1983**, *95*, 579–596. (b) *Angew. Chem., Int. Ed. Engl.* **1983**, *22*, 565−582.
(13) Klug, A. *Philos. Trans. R. Soc. London B* **1999**, *354*, 531–535.
(14) An overview gives: (a) Bong, D. T.; Clark, T. D.; Granja, J. R.; Ghadiri, M. R. *Angew. Chem.* **2001**, *113*, 1016–1041. (b) *Angew. Chem., Int. Ed.* **2001**, *40*, 988−1011.

(15) (a) Percec, V.; Johansson, G.; Ungar, G.; Zhou, J. *J. Am. Chem. Soc.* **1996**, *118*, 9855–9866. (b) Percec, V. *Philos. Trans. R. Soc. London A* **2006**, *364*, 2709–2719.

(16) Peterca, M.; Percec, V.; Dulcey, A. E.; Nummelin, S.; Korey, S.; Ilies, M.; Heiney, P. A. *J. Am. Chem. Soc.* **2006**, *129*, 6713–6728.

(17) Pasternack, R. F.; Gibbs, E. J.; Sibley, S.; Woodard, L.; Hutchinson, P.; Genereux, J.; Kristian, K. *Biophys. J.* **2006**, *90*, 1033–1042.

(18) Schönherr, H.; Paraschiv, V.; Zapotoczny, S.; Crego-Calama, M.; Timmerman, P.; Frank, C. W.; Vancso, G. J.; Reinhoudt, D. N. *Proc. Natl. Acad. Sci. U.S.A.* **2002**, *99*, 5024–5027.

(19) Kawasaki, T.; Tokuhiro, M.; Kimizuka, N.; Kunitake, T. *J. Am. Chem. Soc.* **2001**, *123*, 6792–6800.

(20) van Gorp, J. J.; Vekemans, J. A. J. M.; Meijer, E. W. *J. Am. Chem. Soc.* **2002**, *124*, 14759–14769.

(21) Yagai, S.; Kinoshita, T.; Kikkawa, Y.; Karatsu, T.; Kitamura, A.; Honsho, Y.; Seki, S. *Chem. Eur. J.* **2009**, *15*, 9320–9324.

(22) Jonkheijm, P.; Hoeben, F. J. M.; Kleppinger, R.; van Herrikhuyzen, J.; Schenning, A. P. H. J.; Meijer, E. W. *J. Am. Chem. Soc.* **2003**, *125*, 15941–15949.

(23) Jeukens, C. R. L. P. N.; Jonkheijm, P.; Wijnen, F. J. P.; Gielen, J. C.; Christianen, P. C. M.; Schenning, A. P. H. J.; Meijer, E. W.; Maan, J. C. *J. Am. Chem. Soc.* **2005**, *127*, 8280–8281.

(24) Akutagawa, T.; Ohta, T.; Hasegawa, T.; Nakamura, T.; Christensen, C. A.; Becher, J. *Proc. Nat. Am. Soc.* **2002**, *99*, 5028–5033.

(25) Rapaport, H.; Kim, H. S.; Kjaer, K.; Howes, P. B.; Cohen, S.; Als-Nielsen, J.; Ghadiri, M. R.; Leisterowitz, L.; Lahav, M. *J. Am. Chem. Soc.* **1999**, *121*, 1186–1191.

(26) Fenniri, H.; Deng, B.-L.; Ribbe, A. E. *J. Am. Chem. Soc.* **2002**, *124*, 11064–11072.

(27) Moralez, J. G.; Raez, J.; Yamazaki, T.; Motkuri, R.; Kovalenko, A.; Fenniri, H. *J. Am. Chem. Soc.* **2005**, *127*, 8307–8309.

(28) Jin, W.; Fukushima, T.; Kosaka, A.; Niki, M.; Ishii, N.; Aida, T. *J. Am. Chem. Soc.* **2005**, *127*, 8284–8285.

(29) Balakrishnan, K.; Datar, A.; Zhang, W.; Yang, X.; Tammene, N.; Huang, J.; Zuo, J.; Yen, M.; Moore, J. S.; Zang, L. *J. Am. Chem. Soc.* **2006**, *128*, 6576–6577.

(30) Cheng, X.; Ver Heyen, A.; Mamdouh, W.; Uji-i, H.; De Schryver, F.; Höger, S.; De Feyter, S. *Langmuir* **2007**, *23*, 1281–1286.

(31) Dingenouts, N.; Klyatskaya, S.; Rosenfeldt, S.; Ballauff, M.; Höger, S. *Macromolecules* **2009**, *42*, 5900–5902.

(32) Couet, J.; Biesalski, M. *Small* **2008**, *7*, 1008–1016.

(33) (a) Ghadiri, M. R.; Granja, J. R.; Milligan, R. A.; McRee, D. E.; Khazanovich, N. *Nature* **1993**, *366*, 324–327. (b) Gattuso, G.; Menzer, S.; Nepogodiev, S. A.; Stoddart, J. F.; Williams, D. J. *Angew. Chem.* **1997**, *109*, 1615–1617. (c) *Angew. Chem., Int. Ed. Engl.* **1997**, *36*, 1451−1454.

(34) Sonoda, M.; Yamaguchi, Y.; Tahara, K.; Hirose, K.; Tobe, Y. *Tetrahedron* **2008**, *64*, 11490–11494.

(35) (a) Höger, S.; Ramminger, A.-D.; Rosselli, S.; Wagner, T.; Silier, B.; Wiegand, S.; Häussler, W.; Lieser, G.; Scheumann, V. *Angew. Chem.* **2001**, *113*, 3233–3237. (b) *Angew. Chem., Int. Ed.* **2001**, *40*, 3137−3141. (c) Höger, S.; Rosselli, S.; Ramminger, A.-D.; Wagner, T.; Lieser, G. *Chem. Eur. J.* **2003**, *9*, 3481–3491. (d) Gielen, J. C.; Ver Heyen, A.; Klyatskaya, S.; Vanderlinden, W.; Höger, S.; Maan, J. C.; De Feyter, S.; Christianen, P. C. M. *J. Am. Chem. Soc.* **2009**, *131*, 14134–14135.

(36) Hui, J. K.-H.; Frischmann, P. D.; Tso, C.-H.; Michal, C. A.; MacLachlan, M. J. *Chem. Eur. J.* **2010**, *16*, 2453–2460.

(37) Naddo., T.; Che, Y.; Zhang, W.; Balakrishnan, K.; Yang, X.; Yen, M.; Zhao, Y.; Moore, J. S.; Zang, L. *J. Am. Chem. Soc.* **2007**, *129*, 6978–6979.

(38) Balci, S.; Bittner, A. M.; Hahn, K.; Scheu, C.; Knez, M.; Kadri, A.; Wege, C.; Jeske, H.; Kern, K. *Electrochim. Acta* **2006**, *51*, 6251–6257.

(39) Zhao, D.; Moore, J. S. *Chem. Commun.* **2003**, 807–818.

(40) A polar hydroxy group at the periphery can also favor the aggregation of rigid phenylene−ethynylene rings: Lin, C.-H.; Tour, J. *J. Org. Chem.* **2002**, *67*, 7761–7768.

(41) (a) Brunsveld, L.; Folmer, B. J. B.; Meijer, E. W.; Sijbesma, R. P. *Chem. Rev.* **2001**, *131*, 4071–4097. (b) Ciferri, A. *Supramolecular Polymers*; Marcel Dekker: New York, 2005. (c) Pensec, S.; Nouvel, N.; Guilleman, A.; Creton, C.; Boué, F.; Bouteiller, L. *Macromolecules* **2010**, *43*, 2529−2534.

(42) (a) Milner, S. T. *Science* **1991**, *251*, 905–914. (b) Zhang, M.; Müller, A. H. E. *J. Polym. Sci., Part A: Polym. Chem.* **2005**, *43*, 3461–3481.

(43) No diameter separation procedure is required, compared to carbon nanotubes, which are prepared in a comparably broad diameter distribution, as i.e. described in: Arnold, M. S.; Green, A. A.; Hulvat, J. F.; Stupp, S. I.; Hersam, M. C. *Nature Nanotechnol.* **2006**, *1*, 60–65.

(44) (a) *Polymer Handbook*, 4th ed.; Brandrup, J., Immergut, E. H., Grulke, E. A., Eds.; Wiley-Interscience: New York, 1999; Vol. *2*, pp 300−305. (b) The strong solvent dependence of other aggregating systems and clustering systems is e.g. described in: Jonkheijm, P.; van der Schoot, P.; Schenning, A. P. J. H.; Meijer, E. W. *Science* **2006**, *313*, 80–83.

(45) Mössinger, D.; Chaudhuri, D.; Kudernac, T.; Lei, S.; De Feyter, S.; Lupton, J. M.; Höger, S. *J. Am. Chem. Soc.* **2010**, *132*, 1410–1423.

(46) (a) Ballauff, M.; Li, L.; Rosenfeldt, S.; Dingenouts, N.; Beck, J.; Krieger-Beck, P. *Angew. Chem.* **2004**, *116*, 5967–5970. (b) *Angew. Chem., Int. Ed.* **2004**, *43*, 5843−5846. (c) Walther, A.; Drechsler, M.; Rosenfeldt, S.; Harnau, L.; Ballauff, M.; Abetz, V.; Müller, A. H. *J. Am. Chem. Soc.* **2009**, *131*, 4720–4728.

(47) It is worth mentioning that the introduction of phthalimido groups at the periphery of a shape-persistent macrocycle by treating the macrocyclic diol with phthalimide under Mitsunobu conditions was not successful.

(48) (a) Höger, S.; Meckenstock, A.-D.; Pellen, H. *J. Org. Chem.* **1997**, *62*, 4556–4557. (b) Höger, S.; Meckenstock, A.-D. *Tetrahedron Lett.* **1998**, *39*, 1735–1736. (c) Höger, S. *Macromol. Symp.* **1999**, *142*, 185–191.

(49) Balagurusamy, V. S. K.; Ungar, G.; Percec, V.; Johansson, G. *J. Am. Chem. Soc.* **1997**, *119*, 1539–1555.

(50) Höger, S.; Bonrad, K.; Mourran, A.; Beginn, U.; Möller, M. *J. Am. Chem. Soc.* **2001**, *123*, 5651–5659.

(51)

$$\delta = \delta_0 + (\delta_\infty - \delta_0)\left(\frac{4KM_{\mathrm{tot}} + 1 - \sqrt{8KM_{\mathrm{tot}} + 1}}{4KM_{\mathrm{tot}}}\right)$$

(52) Provencher, S. W. *Biophys. J.* **1976**, *16*, 27–41.

(53) The observation of only one species with a rather small hydrodynamic radius might be the result of a specific dimerization where the macrocycles are arranged face-to-face and rotated by 90°, so that the dendritic side groups efficiently block the top and bottom of the dimer and prevent a further growth of the aggregate. A similar observation has been made on other macrocycles. Cf.: Klyatskaya, S.; Dingenouts, N.; Rosenauer, C.; Müller, B.; Höger, S. *J. Am. Chem. Soc.* **2006**, *128*, 3150–3151.

(54) Higgins, J. S.; Benoit, H. C. *Polymers and Neutron Scattering*; Clarendon: Oxford, 1994.

(55) The (outer) radius, R, is larger than the radius of gyration perpendicular to the cylinder axis, R_c, due to the definition of the radius of gyration.

(56) The deconvolution was performed as following: A local mean filter was applied, calculating the average height of an area of 21^2 nm^2 around each pixel, resulting in an averaged topography image. This image, in which only raw features are visible, is subtracted from the original topography data, yielding the enhanced visibility of the small features in the <20 nm size regime. The deconvolution was done with the SPIP software package, ImageMetrology.

(57) As mentioned before, even after this storage time, no precipitation of the tubes from the solution could be observed, as it should happen if the network shown in Figure 6d would already exist in solution.

(58) Lateral dimensions (i.e., widths) of individual objects are typically overestimated by AFM due to a limited tip radius and an interaction range being typically larger than the measured dimensions. However, the width of particles within a periodic lattice is measured correctly via the lattice distance. For further details see, e.g.: García, R.; Pérez, R. *Surf. Sci. Rep.* **2002**, *47*, 197–301.

(59) In particular, as soft tapping conditions (i.e., small free amplitude and small damping) are chosen, the determined heights represent a good approximation for the tube diameter. Noteworthy, the force applied by the AFM tip in the amplitude-mode (AM) exerts a certain pressure on the sample and may cause a deformation of soft matter (cf.: Yang, C. W.; Hwang, I.-S.; Chen, Y. F.; Chang, C. S.; Tsai, D. P. *Nanotechnology* **2007**, *18*, 084009). Additionally, the influence of the substrate/molecule interaction on the tube cross section is not clear at present. Cf.: Djalali, R.; Li, S.-Y.; Schmidt, M. *Macromolecules* **2002**, *35*, 4282–4288. Börner, H. G.; Beers, K.; Matyjaszewski, K.; Sheiko, S. S.; Möller, M. *Macromolecules* **2001**, *34*, 4375–4383.

(60) For self-assembled monolayers of phenylene−ethynylene−butadiynylene macrocycles on HOPG see: (a) Höger, S.; Bonrad,

K.; Mourran, A.; Beginn, U.; Möller, M. *J. Am. Chem. Soc.* **2001**, *123*, 5651–5659. (b) Borissov, D.; Ziegler, A.; Höger, S.; Freyland, W. *Langmuir* **2004**, *20*, 2781–2784. (c) Tahara, K.; Johnson, C. A., II; Fujita, T.; Sonoda, M.; De Schryver, F. C.; De Feyter, S.; Haley, M. M.; Tobe, Y. *Langmuir* **2007**, *23*, 10190–10197. (d) Lei, S.; Tahara, K.; De Schryver, F. C.; Van der Auweraer, M.; Tobe, Y.; De Feyter, S. *Angew. Chem.* **2008**, *120*, 3006–3010. (e) *Angew. Chem., Int. Ed.* **2008**, *47*, 2964−2968. (f) Jester, S.-S.; Shabelina, N.; Le Blanc, S. M.; Höger, S. *Angew. Chem.* **2010**, *122*, 6237–6241. (g) *Angew. Chem., Int. Ed.* **2010**, *49*, 6101−6105.

(61) At the present stage, we assume that different interaction strengths (as discussed above) lead to unlike adsorption behavior of aggregates of **2a** on substrates that are different in polarity or able to support commensurate adlayers due to specific interatomic distances of the surface crystal lattice. Additionally, contact electrification can be discussed as an origin for the adsorbate−substrate interaction for the particular case of polystyrene on HOPG. The term "contact electrification" describes electrical charging of PS on a HOPG surface due to accessibility of respective acceptor states in PS from the Fermi level of HOPG. (see, e.g.: Gady, B.; Reifenberger, R.; Rimai, D. S. *J. Appl. Phys.* **1998**, *84*, 319–322). However, presently the role of contact electrification on the quantitative description of the adsorbate−substrate interactions of aggregates of **2a** with HOPG is unclear.